Three-Dimensional Simulations of Plate Anchor Pullout in Granular Materials

T. Matthew Evans, Ph.D., A.M.ASCE[1]; and Nan Zhang, Ph.D.[2]

Abstract: Plate anchors are embedded into the ocean floor to provide holding capacity for offshore structures. Anchor holding capacity is a function of both the anchor and soil properties. Although plate anchors have been widely studied experimentally and numerically, there is still no universally agreed-upon design approach, indicating that the problem physics remain elusive. In this work, discrete-element method (DEM) simulations were used to investigate the behavior of plate anchors during pullout in an effort to elucidate some of the microscale physical processes that influence overall system behavior. Macroscale assembly response was compared to published experimental results and empirical solutions. The influence of embedment ratio, anchor roughness, soil density, and anchor size on holding capacity was investigated, and system-scale results reasonably agreed with previously published work. Thus, observations of the simulated contact force network and particle velocity during uplift were used to provide insight into anchor failure mechanisms. Finally, the model was used to briefly explore the response of a cyclically loaded plate anchor embedded in a granular assembly. **DOI: 10.1061/(ASCE)GM.1943-5622.0001367.**

Author keywords: Plate anchor; Breakout factor; Pullout force; Failure mechanism; Contact force network.

Introduction

For structures such as transmission towers, earth retaining walls, and offshore structures [e.g., wave energy converters (WECs)], an anchoring system is often critical to provide holding capacity and maintain stability. The functions of anchoring systems in engineering applications are to withstand environmental loading and keep structures in position. Plate anchors are a type of anchor commonly used in ground and offshore applications. Offshore plate anchors can be slotted into the toe end of a suction caisson. The suction caisson is embedded into the seabed, then withdrawn, leaving the plate anchor embedded (Valent et al. 1979; Gaudin et al. 2006; Randolph and Gourvenec 2011).

Prior studies of plate anchors have been widely reported in the literature. Physical experiments, model tests, and analytical approaches have been used to study the behavior of plate anchors. These studies considered anchor behaviors as a function of a variety of variables, including embedment depth, soil density, anchor roughness, and soil type, and have shown that anchors respond to loading in a manner similar to that of foundation structures observed in bulk soils and other geostructures. Most of the previous research has focused on experimental and continuum numerical analyses. Physical experiments are used to evaluate anchor behavior and the influence of soil properties on holding capacity; prior numerical simulations have been largely predicated on the assumption of soil as a continuum.

Meyerhof and Adams (1968) conducted uplift tests as part of a study on transmission tower footings. Model tests were compared with the full-scale tests, and complex failure mechanisms were observed to vary with the depth of foundation embedment. Based on the model tests, a semianalytical relationship based on shape and depth was developed to compute full-scale uplift capacity. Vesić (1971) used cavity expansion theory to study factors affecting the force magnitude necessary to cause full withdrawal of objects from the ocean bottom and found that the relative depth of embedment and soil type were the primary influencers of breakout force.

Many prior studies on plate anchors have focused on seeking a dimensionless factor (e.g., breakout factor, uplift coefficient, dimensionless load coefficient) to describe anchor holding capacity (Meyerhof and Adams 1968; Das and Seeley 1975; Murray and Geddes 1987) and critical embedment depth for varying failure mechanisms. One common dimensionless factor (breakout factor) has been defined as the maximum holding resistance normalized by the weight of soil above the plate anchor. The critical embedment depth is the point of transition where the breakout factor does not continue to increase with increasing embedment depth and corresponds to a transition point ranging from a shallow failure mechanism (defined as a ratio of embedment depth to anchor width of less than 5.0) to a deep failure mechanism. The critical embedment depth depends on the peak angle of shearing resistance, which in turn is related to soil density (Holtz et al. 2011).

Das and Seeley (1975) used physical experiments to measure the breakout resistances of rectangular plate anchors. The breakout resistance of shallow anchors embedded into loose soil was studied to develop breakout factors and critical depths of embedment for varying length-to-width ratios. Rowe and Davis (1982) theoretically investigated the behaviors of anchor plates in sand, considering anchor embedment ratio, soil friction angle and dilatancy, initial stress state, and anchor roughness. They showed that anchor roughness affected capacity in the case of a vertical anchor. Subsequent work by Murray and Geddes (1987) used limit equilibrium analyses to predict the ultimate pullout resistance of plate anchor model tests and found that anchor roughness had a negligible effect on capacity.

[1]Associate Professor, School of Civil and Construction Engineering, Oregon State Univ., 101 Kearney Hall, Corvallis, OR 97331. Email: matt.evans@oregonstate.edu

[2]Graduate Research Assistant, School of Civil and Construction Engineering, Oregon State Univ., 101 Kearney Hall, Corvallis, OR 97331 (corresponding author). Email: zhangn@oregonstate.edu

Note. This manuscript was submitted on January 5, 2018; approved on September 7, 2018; published online on January 14, 2019. Discussion period open until June 14, 2019; separate discussions must be submitted for individual papers. This paper is part of the ***International Journal of Geomechanics***, © ASCE, ISSN 1532-3641.

In both studies, however, soil dilatancy was shown to significantly increase the anchor capacity (Rowe and Davis 1982; Murray and Geddes 1987). Chattopadhyay and Pise (1986) presented a theoretical model that assumed a curved failure surface through the soil to evaluate the ultimate breakout resistance of horizontal plate anchors for sands with a wide range of shear strengths. Dickin (1988) performed centrifuge uplift tests of rectangular plate anchors of varying anchor geometry, embedment depth, and soil density. Failure displacements were reported to increase with embedment but reduce with an increase in soil density or anchor aspect ratio. Overall, the aforementioned studies demonstrated that anchor holding capacity is sensitive to soil density, soil dilatancy, and embedment depth but relatively insensitive to anchor roughness and geometry and, in certain cases, initial state (K_0).

Rao and Kumar (1994) developed a semianalytical equation by assuming a log-spiral failure surface and accounting for the effects of cohesion; surcharge load; and soil density, embedment depth, and friction angle. This assumed failure surface produced reasonable predictions of anchor pullout behavior in loose to medium-dense sands. Basudhar and Singh (1994) first reported a lower-bound solution for horizontal and vertical strip anchors embedded into sand. Subsequently, Merifield and Sloan (2006) used upper-bound and lower-bound limit analyses and finite-element analyses to estimate anchor breakout factors and soil displacements with various embedment depths and soil friction angles. The failure mode was found to be an upward rigid column moving from the anchor to the soil surface. Anchor roughness was found to have little or no effect on pullout capacity. Kumar and Kouzer (2008a, b) also performed upper-bound limit analyses and finite-element analyses and considered the plastic strain of all elements with varying embedment ratio and friction angle. The breakout factor was found to increase with increasing embedment ratio and friction angle.

Prior research has provided an understanding of the constitutive behavior of plate anchors and the variables that govern response. Analytical, empirical, and experimental investigations of anchor behavior instruct the practice of design. However, there are still discrepancies between analytical and empirical predictions and model measurements; microscale insights into system response during anchor pullout can help to inform these existing approaches. This paper presents results from discrete-element method (DEM) simulations of the behavior of embedded plate anchors during uplift in granular soils. DEM allows for the simulation of soils as a discontinuous medium (Cundall and Strack 1979) and has been applied to a wide range of problems involving granular materials interacting with structures (e.g., Frost et al. 2002; Kress and Evans 2010; Evans and Kress 2011; Zhang and Evans 2016, 2017, 2018; Zhao et al. 2017, 2018; Gao and Meguid 2018). DEM models predict the emergent behavior of particulate assemblies (e.g., sands) based on simulation of independent particle behaviors. Athani et al. (2017) used DEM to conduct two-dimensional simulations of plate anchors embedded into granular soils, specifically considering the influence of the ratio of embedment depth to anchor width and grain size on the holding capacity. They found that the anchor width to grain size ratio and internal friction angle influenced the uplift capacity of the plate anchor. The breakout factor increased linearly with increasing ratio of grain size to anchor width (d:B). However, when d:B was very small, the grain size was found to contribute negligibly for anchors in sandy soils.

In marine systems, the interaction between seabed sands and offshore anchors is one specific example of soil–structure interaction. The properties of the seabed and the anchor combine to determine the holding capacity and allowable reaction force for a given anchor design. Most previous research on plate anchors has been based on physical experiments and analytical modeling, such as limit equilibrium (e.g,. Meyerhof and Adams 1968; Murray and Geddes 1987; Dickin 1988). However, many of the microscale behaviors that occur at the anchor–soil interface are not considered when assessing the holding capacity of a plate anchor and the extensibility of given findings to another situation (e.g., different soil conditions). The current work used DEM simulations utilizing the software PFC^{3D} (Itasca Consulting Group 2008) to evaluate the effects of soil properties and anchor surface roughness on holding capacity and to investigate the micromechanics of anchor uplift. By better understanding the fundamental particle-scale soil response during uplift, it may be possible to better extrapolate results from physical experiments to a wider variety of anchor–seabed combinations.

Simulation of Plate Anchor

Model Overview

The DEM model consisted of spherical particles and boundary walls. The model geometry is presented in Fig. 1. An assembly of polydisperse spherical particles was generated to fill the model volume in the box at a user-defined porosity. The model variables and material properties are presented in Table 1. A linear spring contact model (e.g., Cundall and Strack 1979; Itasca Consulting Group 2008; O'Sullivan 2011) was used in the simulations. Particle–particle and particle–wall contacts were considered as springs in the normal and shear direction. Particles were assigned normal and shear stiffnesses to produce a load-displacement response similar in magnitude to the nonlinear Hertz-Mindlin contact model. In general, material properties were selected to be consistent with physical properties of silica sands previously published in the literature. However, it is possible to vary these parameters to simulate other soil types (e.g., carbonate sands) or to calibrate the model to the observed response while remaining within the range of physically realistic material properties.

Previous research on the shear strength of granular soils has shown that shear band thickness is approximately 10–12 times the median particle diameter (e.g., Mühlhaus and Vardoulakis 1987; Frost et al. 2004). Thus, the distance between the edges of the plate anchor and outside walls was set as $19.5d_{50}$ (where d_{50} is the mean model particle diameter) to allow sufficient space for shear bands to fully form around the anchor plate. According to Dickin (1988), the soil beneath the anchor has little influence on the anchor capacity, so the distance between plate anchor and bottom wall was set to a relatively small value for computational efficiency. Seafloor sands are porous materials with generally high permeabilities, so suction forces below the plate anchor during pullout are not considered (Das et al. 1994). Finer-grained materials would require a coupled hydromechanical treatment. Different embedment depths can be modeled by changing the vertical position of the plate in the simulations.

Mass scaling (e.g., Belheine et al. 2009; Zhao and Evans 2009; Evans and Valdes 2011) was used to decrease simulation time; as such, the mean model particle diameter was $d_{50} = 0.5$ m, and other model dimensions were scaled accordingly. Specifically, model height (H), model width (W), and model length (L) can be expressed in terms of d_{50} as $H = 40d_{50}$ and $W = L = 44d_{50}$. The plate anchor was modeled as a rigid monolayer of small particles arranged on a simple cubic lattice. As seen in Fig. 1, the diameter of the plate anchor particles was $d = 0.2d_{50}$. Note that plate anchor roughness (defined as the mean peak-to-valley distance) was solely defined by the plate anchor particle diameter. The plate

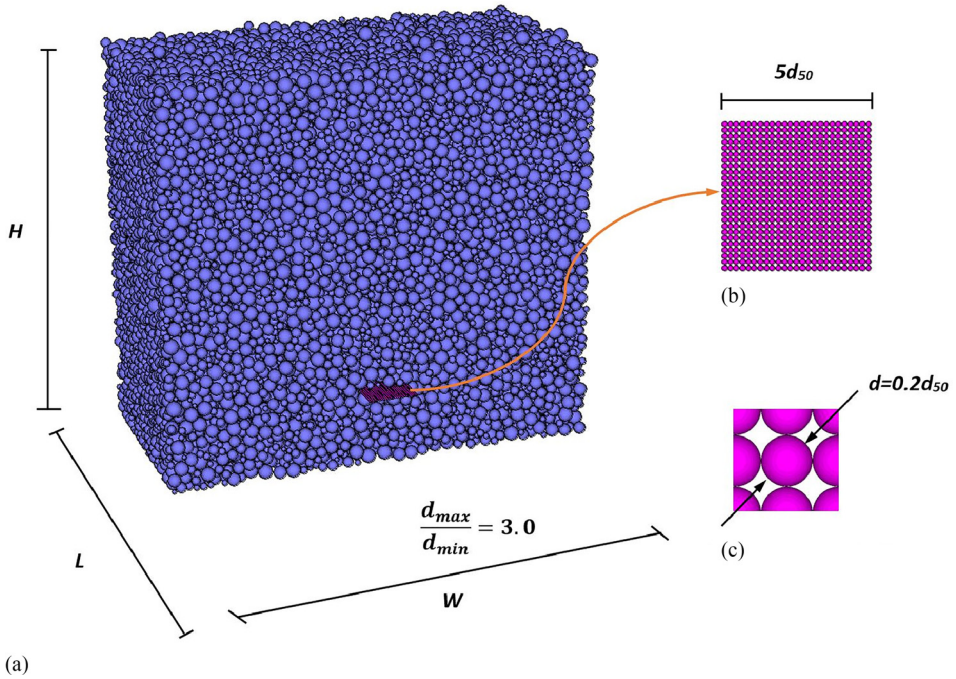

Fig. 1. DEM model: (a) granular assembly; (b) plate anchor; and (c) plate anchor ball. Particle assembly presented in section with half of particles was removed to reveal embedded plate anchor.

Table 1. Material and model properties

Parameter	Value
Particles	
Particle diameter ratio[a] (d_{max}/d_{min})	3
Normal stiffness [k_n (N/m)]	1×10^8
Shear stiffness [k_s (N/m)]	8×10^7
Friction coefficient (μ)	0.50
Specific gravity (G_s)	2.65
Density [ρ_s (kg/m^3)]	2,650
Model	
Height [H (d_{50})]	40
Width [W (d_{50})]	44
Length [L (d_{50})]	44
Wall stiffness [k_w (N/m)]	2×10^8
Gravity (m/s^2)	0.981
Plate anchor	
Normal stiffness [k_{pn} (N/m)]	1×10^8
Shear stiffness [k_{ps} (N/m)]	8×10^7
Particle diameter [d (d_{50})]	0.02
Width [w (d_{50})]	5
Length [l (d_{50})]	5

[a]Particle diameters are uniformly distributed between d_{min} and d_{max}.

anchor had dimensions of $5d_{50} \times 5d_{50} \times 0.2d_{50}$ ($\approx 0.114W \times 0.114L \times 0.005H$).

A numerical servocontrol mechanism was used to isotropically consolidate the specimen by moving the boundary walls such that it was in numerical equilibrium at a specified isotropic stress state within a tolerance of 0.5%. The porosity of the consolidated assembly could be adjusted by varying the particle and wall friction coefficients during assembly generation and consolidation, with a lower friction coefficient resulting in a denser specimen. After consolidation, particle friction was adjusted to the desired value for the material being simulated (but could not be less than the value used for consolidation because the contact network would collapse). The top wall was removed to model uplift in soils with a free surface. The specimen was then re-equilibrated, and finally, a constant upward velocity was applied to the anchor plate while the remaining specimen boundaries remained fixed. To monitor system response during anchor uplift, 100 spherical measurement regions were generated at random locations within the specimen, each having a diameter of twice the maximum particle size ($2d_{max}$). (Note that these measurement spheres were simply convenient regions over which model response could be averaged.) The anchor holding capacity was the out-of-balance force on the plate anchor.

Fig. 2. Anchor roughness.

Parametric Analyses

A total of 16 simulations were performed to investigate the uplift behavior of a plate anchor considering variations in embedment depth, void ratio of the assembly, anchor size, and anchor roughness. Three triaxial shear simulations were performed to measure the bulk shear strength of the simulated material. The embedment ratio was defined as the embedment depth normalized by anchor width ($\lambda = H_0/B$), where H_0 is the embedment depth, and B is the anchor width. The considered embedment ratios varied from 1.6 to 7.2. Anchor sizes ranged from $5d_{50}$ to $7d_{50}$. We defined anchor roughness as the peak-to-valley distance on the anchor surface (i.e., the particle radius in this case). Therefore, anchor roughness may be varied by using different anchor particle sizes. As the size of the particles that comprised the plate anchor increased, so did the tip-to-trough distance of the surface (Fig. 2). Using the surface roughness measure proposed by Uesugi and Kishida (1986), anchor surface roughness varied from $0.1d_{50}$ to $1.0d_{50}$ as the anchor particle

diameter increased from $0.1d_{50}$ to $1.0d_{50}$. Assembly void ratios ranged from 0.539 for relatively dense assemblies to 0.661 for relatively loose assemblies.

A quantity typically referred to as the breakout factor [N_γ, sometimes referred to as the dimensionless load coefficient (Murray and Geddes 1987) or capacity factor (Meyerhof 1951; Meyerhof and Adams 1968)] is commonly used as a quantitative measure of anchor holding capacity (Das and Seeley 1975; Dickin 1988; Murray and Geddes 1989; Dickin and Laman 2007). The breakout factor is a unitless quantity defined as peak uplift resistance normalized by the gravitational force applied to the anchor by the overburden material, as presented in Eq. (1)

$$N_\gamma = \frac{P_{\text{peak}}}{\gamma A H_0} \tag{1}$$

where P_{peak} = peak resistance; γ = unit weight of the overlying material; H_0 = embedment depth; and A = planar area of the anchor.

Results and Discussion

We considered both the specimen-scale and discrete information obtained via DEM simulations to investigate system response as a function of the factors described earlier. Understanding the basic physics of material response during anchor loading can provide insight into uplift behavior in practice. We considered each parametric variable individually.

Material Shear Strength

Many existing design approaches for plate anchors rely upon knowledge of the shear strength of the material in which the anchor is embedded. Thus, to aid comparison between the DEM simulations described herein and results from physical and analytical studies reported in the literature, it is necessary to know the shear strength of the model granular material.

The internal friction angle of the granular assembly was obtained through simulation of triaxial compression element tests using the same parameter values used in the plate anchor uplift simulations (i.e., Table 1). Three triaxial simulations with different confining stresses were used to define the Mohr-Coulomb failure envelope at critical state (Fig. 3). The granular material was found to have an internal friction angle of $\phi' = 24°$.

Embedment Ratio (λ)

Eight different embedment ratios were simulated to investigate the influence of embedment depth on anchor pullout capacity while the other simulation parameters (e.g., stress state and void ratio of the assembly) remained constant. The anchor resistance factor (N), the peak value of which is defined as the breakout factor, was used to describe the magnitude of anchor resistance

$$N = \frac{R}{\gamma A H_0} \tag{2}$$

where R = anchor resistance; and the other terms are as previously defined.

Fig. 4 presents the anchor resistance factor versus displacement for each embedment ratio. The maximum anchor resistance factor (i.e., breakout factor) increased with increasing embedment ratio. A larger embedment ratio implies greater soil weight above the anchor and a larger holding capacity when multiplied by the relatively

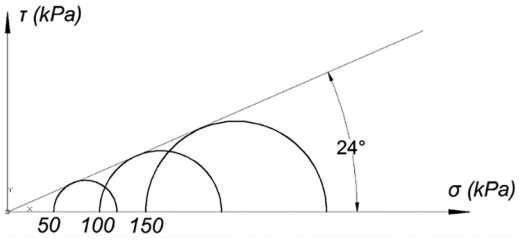

Fig. 3. Mohr's circles at failure for axisymmetric compression tests on the model material at three different confining stresses.

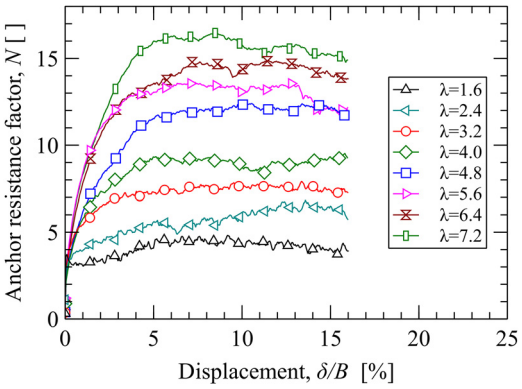

Fig. 4. Anchor resistance factor as a function of displacement.

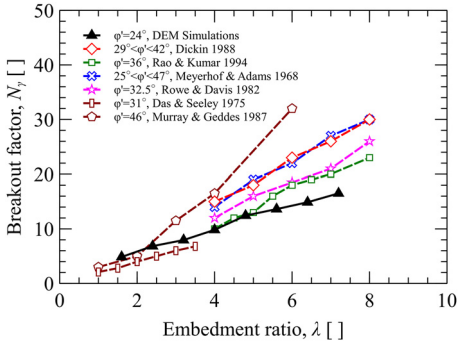

Fig. 5. Comparisons of breakout factors along with embedment ratio between experimental tests and DEM simulation.

larger breakout factor. Breakout factors ranged from 5 to 17 as λ increased from 1.6 to 7.2 for the assembly of particles, which is consistent with results from physical experiments (e.g., Meyerhof and Adams 1968; Rowe and Davis 1982; Dickin 1988).

Comparisons to physical experiments reported in the literature can be used to evaluate the DEM model. Square anchor plate pullout tests performed by Meyerhof and Adams (1968), Das and Seeley (1975), Rowe and Davis (1982), Murray and Geddes (1987), Dickin (1988), and Rao and Kumar (1994) were used for comparison. In general, the breakout factor varies linearly with embedment ratio, although the slope of this relationship varies from study to study. Results from the DEM simulations were consistent with and in a similar range as the experimental results reported by the previously listed researchers (Fig. 5).

The DEM simulation results were most consistent with the tests performed by Das and Seeley (1975) and Rao and Kumar (1994). All of the results showed the breakout factor linearly increasing as a function of embedment ratio. When the embedment ratio varied

from 1 to 8, N_γ ranged from 2 to 30. However, none of the experiments reached the critical embedment ratio or critical breakout factor. Note that the critical embedment ratio is a limiting value; once it is reached, the breakout factor is also a constant limiting value (i.e., the critical breakout factor). This implies that the anchor embedment depth is significantly important in determining holding capacity.

Consistent with the prediction by Meyerhof and Adams (1968), the mass of soil displaced at the ultimate uplift load was shaped like a conical frustum. For the shallow anchors, the failure surface reached the ground surface. Fig. 6 presents particle velocity vectors for the shallowest anchor. Three dashed lines indicate the range of potential inclinations of the implied failure surface ($\phi'/3$, $\phi'/2$, and ϕ'). Note that there was no consistency in the failure surface inclinations published in the literature. From prior research, the inclination of failure surface (θ) generally ranges from $\phi'/3$ to ϕ'; for instance, Murray and Geddes (1987) reported that $\phi'/2 \leq \theta \leq \phi'$, whereas Dyson and Rognon (2014) reported that $\phi'/2 \leq \theta \leq 2\phi'/3$, and Meyerhof and Adams (1968) found that $\theta = \phi'/3$.

Meyerhof and Adams (1968) found that the ultimate uplift load of a square plate anchor is similar to that of a circular plate anchor. The shearing resistance of the square plate anchor is the mobilization of passive earth pressure inclined at an angle (θ) on a quadrangular pyramidal frustum through the anchor edges. They found that the ultimate uplift load for a shallow anchor can be computed by

$$Q_u = \pi c B H_0 + s\pi B \frac{\gamma {H_0}^2}{2} K_u \tan\phi' + W \tag{3}$$

where B = anchor width/length; H_0 = embedment depth; s = empirical shape factor; K_u = nominal uplift coefficient of earth pressure on a vertical plane; and W = anchor weight. For granular soils, c is zero and the equation simplifies to

$$Q_u = s\pi B \frac{\gamma {H_0}^2}{2} K_u \tan\phi' + W \tag{4}$$

The theoretical relationships between the angle of internal friction and the shape factor (s) and K_u have been reported by Meyerhof and Adams (1968) and are shown in Figs. 7 and 8, respectively. From Fig. 7, the shape factor was $s = 1.25$ for a friction angle of 24° (Fig. 3). Similarly, according to Fig. 8, K_u = 0.88 for the granular assembly considered herein (K_{pv} and K_u are related by $K_{pv} = K_u \tan\phi'$). The breakout factor may then be expressed as

$$N_\gamma = \frac{Q_u}{\gamma z_e A} = \frac{s\pi B \frac{\gamma {H_0}^2}{2} K_u \tan\phi' + W}{\gamma H_0 B^2} \tag{5}$$

In the current simulations, the anchor weight was very small and may be neglected, resulting in

$$N_\gamma = \frac{s\pi\lambda K_u \tan\phi'}{2} \tag{6}$$

The breakout factor, as calculated from Eq. (6), is a linear function of the embedment ratio (λ). The rate of increase is determined by the shape factor, the nominal uplift coefficient of earth pressure on a vertical plane, and the internal friction angle of the soil.

Ovesen (1981) reported an empirical formula for the breakout factor for shallow anchors ($1 \leq \lambda \leq 3.5$) and internal friction angles between 29 and 42°

$$N_\gamma = 1 + \left(4.32\tan\phi' - 1.58\right)\lambda^{3/2} \tag{7}$$

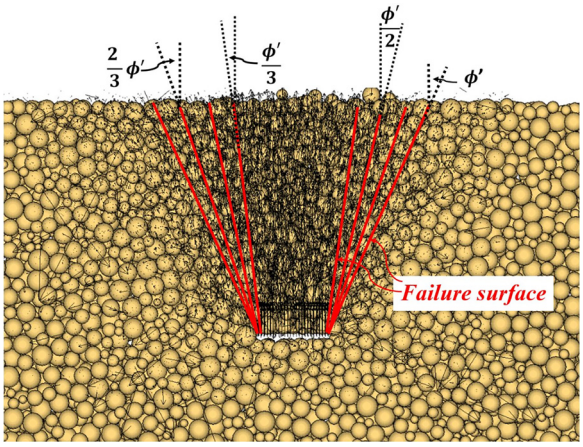

Fig. 6. Velocity vectors for granular assembly with a fully mobilized shallow plate anchor. Dashed lines indicate failure surface inclinations of $\phi'/3$, $\phi'/2$, $2\phi'/3$, and ϕ'.

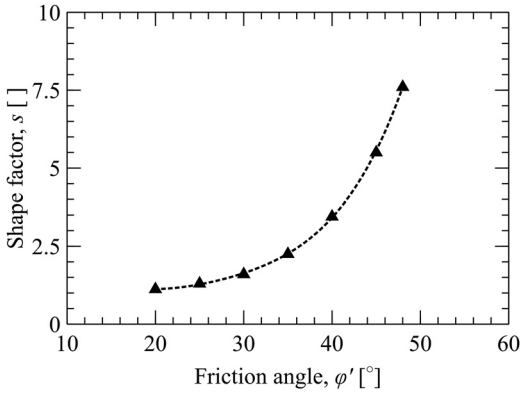

Fig. 7. Meyerhof and Adams (1968) shape factors as a function of soil friction angle.

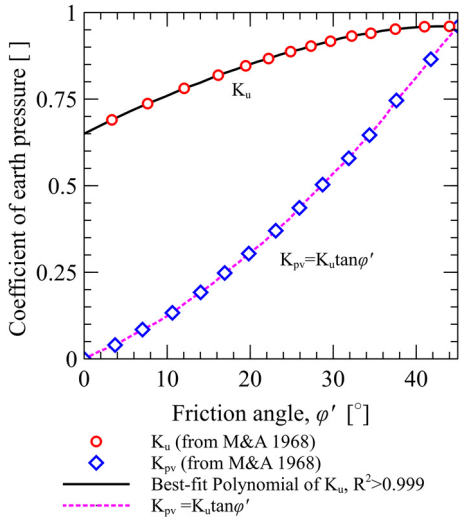

Fig. 8. Theoretical uplift coefficient of earth pressure. Data points are digitized from the curves of Meyerhof and Adams (1968). A polynomial is fit to the K_u data (solid line, $R^2 > 0.999$) and then used to predict the K_{pv} data using the relationship $K_{pv} = K_u \tan\phi'$ (dashed line) as a check on the quality of digitization.

Referring to the nominal uplift coefficient of earth pressure on vertical plane (K_u) proposed by Meyerhof and Adams (1968) and results from physical experiments, Das and Seeley (1975) proposed an equation for the breakout factor of a rectangular anchor embedded in a granular soil with $\phi' = 31°$ (square anchor is a special case)

$$N_\gamma = 2\lambda s K_u \tan\phi' + 1 = 2\lambda s K_{pv} + 1 \tag{8}$$

Dyson and Rognon (2014) also developed an equation for the breakout factor

$$N_\gamma = \frac{1}{3}\left[(1 + 2\lambda\tan\theta)^2 + 2\lambda\tan\theta + 2\right] \tag{9}$$

where θ ranges from $\phi'/2$ to $2\phi'/3$. The upper-bound solution for a circular anchor derived by Murray and Geddes (1987) is shown in Eq. (10)

$$N_\gamma = 1 + 2\lambda\tan\phi'\left(1 + \frac{2}{3}\lambda\tan\phi'\right) \tag{10}$$

Murray and Geddes (1987) also developed a solution for rectangular plate anchors [Eq. (11)] in which the square plate anchor is a specific case

$$N_\gamma = 1 + 2\lambda\tan\phi'\left(1 + \frac{\pi}{6}\lambda\tan\phi'\right) \tag{11}$$

The dimensionless breakout factors from these equations for an internal friction angle of 24° and that measured in the DEM simulations are presented in Fig. 9. Breakout factors calculated using approaches previously reported in the literature are typically functions of only internal friction angle and/or embedment ratio, except for that proposed by Dyson and Rognon (2014), which requires specification of failure surface inclination. Fig. 9 presents breakout factors calculated using both the upper- and lower-bound failure surface inclinations identified by Dyson and Rognon (2014).

Of the relationships presented in Fig. 9, the DEM simulations generally predicted higher breakout factors compared to the empirical results for the same friction coefficient. Development (and, in some cases, calibration) of the semianalytical breakout equations involves assumptions about the failure mechanism and failure wedge geometry. When in doubt, conservative assumptions are typically used, and often there are few data available for calibration. Thus, the semianalytical approaches are likely inherently conservative. Furthermore, the specific ranges of friction angles over which the empirical equations remain valid are not generally well defined. Even though Fig. 9 presents the empirically calculated breakout factors using the embedment ratios and friction angle from the DEM simulations, the empirical solutions may not be strictly applicable for lower angles of internal friction [e.g., recall that the Das and Seeley (1975) equation was developed for a single soil with $\phi' = 31°$]. This is likely the reason that the DEM simulation results were most consistent with the upper-bound solution of Murray and Geddes (1987). Importantly, the breakout factors from the DEM simulations were in much better agreement with the experimental results and model tests presented in Fig. 5 than with the empirical predictions. Nonetheless, the breakout factor obtained from the DEM simulations exhibited a rate of increase with increasing embedment ratio that was similar to the empirical predictions.

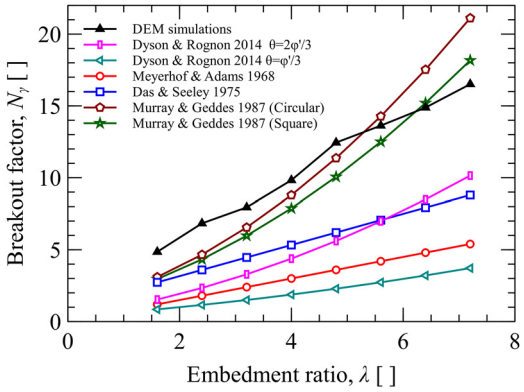

Fig. 9. Breakout factor as a function of embedment ratio (DEM versus semianalytical solutions).

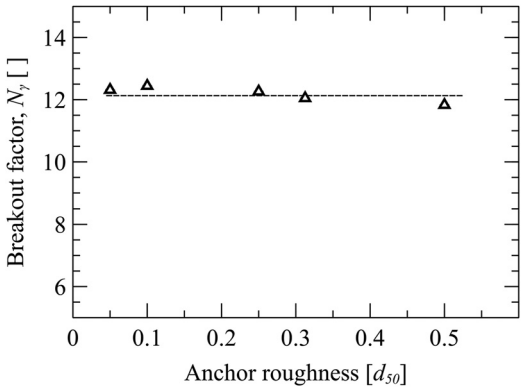

Fig. 10. Anchor resistance as a function of anchor surface roughness ($\lambda = 4.8$).

Anchor Roughness

A given surface can largely be defined by its stiffness, hardness, and roughness. Of these three factors, roughness will vary over the largest range for different anchor materials, particularly if surface evolution over the system's lifetime is considered. To assess the effects of changing plate anchor roughness, simulations were performed using an embedment ratio of 4.8 with varying anchor particle diameters of 0.100, 0.200, 0.500, 0.625, and $1.00d_{50}$. The corresponding anchor roughnesses were then 0.050, 0.100, 0.250, 0.313, and 0.500, as defined earlier. Fig. 10 presents the breakout factor for different anchor roughnesses at the same embedment ratio ($\lambda = 4.8$). The breakout factors varied over a narrow range from 11.8 to 12.4 as roughness varied. The results imply that anchor roughness has little influence on the resistance of plate anchors. This is reasonable, given that anchor resistance is primarily due to the soil weight above the plate anchor and Coulomb's force along the shearing surface. This finding is consistent with those reported by several other researchers (e.g., Rowe and Davis 1982; Song et al. 2008; White et al. 2008; Yu et al. 2011), not only experimentally but also numerically. If a perfectly smooth (and frictionless) anchor was simulated, we would expect capacity to decrease because the rigid wedge immediately above the anchor would not form and soil could more freely flow around the anchor as it moves. The current results show that only a small amount of roughness (in addition to the anchor friction) is necessary to allow the rigid wedge to form, and that further increases in roughness do not serve to alter pullout response.

Soil Density

Soil density can be adjusted by varying the particle friction coefficients during assembly generation and consolidation, with a lower

friction coefficient resulting in a denser specimen and higher friction coefficients resulting in a looser specimen. To study the effects of soil density on pullout resistance, a set of simulations with void ratios ranging from $e = 0.539$ to $e = 0.661$ were considered. The anchor resistance factor (N) as a function of relative displacement for different void ratios is presented in Fig. 10. As expected, these results indicate that denser assemblies have a greater pullout resistance.

Fig. 11 indicates that the densest assembly experienced strain softening during anchor uplift. For looser assemblies, a well-defined peak anchor resistance was not obvious. There was no strain softening for the loosest assemblies; instead, the anchor resistance factor increased gradually to a relatively constant value. The anchor resistance factor exhibited postpeak strain softening when the granular assembly was very dense ($e = 0.539$). The anchor resistance factor increased to a peak value and then decreased due to the failures along the truncated cone failure surface. Particle sliding, rotation, and possibly crushing would occur along the failure surface, resulting in the postpeak decrease in anchor holding capacity. However, anchor resistance in the loosest assembly ($e = 0.661$) exhibited strain-hardening behavior because anchor mobilization will densify the assembly above the plate anchor. Fig. 12 presents breakout factors as a function of void ratio. The relationship was approximately linear from a value of $N_\gamma = 5$ for the loosest assembly to $N_\gamma = 12$ for the most dense. Soil density clearly had a significant effect on anchor holding capacity.

Fig. 13 compares the breakout factor as a function of embedment ratio for both dense and loose assemblies. In the range of embedment ratios considered, the breakout factor increased linearly with embedment ratio for dense assemblies. However, the breakout factor had a bilinear relationship with the embedment ratio for loose assemblies, initially increasing with embedment up to some critical embedment ratio ($\lambda = 5.8$ in our simulations), after which it remained constant. This phenomenon has also been found experimentally (Vesić 1971; Das and Seeley 1975) and theoretically (Chattopadhyay and Pise 1986). The critical embedment depth depends on the angle of internal friction. As found through DEM simulations and reported by previous researchers, the critical embedment ratio increased with internal friction and decreased with void ratio (Meyerhof and Adams 1968; Das and Seeley 1975; Dickin 1988; Frydman and Shaham 1989; Rao and Kumar 1994; Ilamparuthi et al. 2002). The critical breakout factors reported here ranged from 5 to 12 for rectangular plate anchors. Thus, the results from the DEM simulations presented in Fig. 13 were consistent with the results presented in the literature.

Plate anchor movement will mobilize the overlying granular material. Particles in contact with the plate anchor serve to transmit forces from the displacing plate to the remainder of the assembly. Fig. 14 presents the contact force networks of plate anchors at two embedment ratios for both a dense ($e = 0.590$) and a loose ($e = 0.625$) assembly. The contact force networks had an inverted *root-like* structure with larger forces contacting the plate anchor that attenuated to smaller contact forces as the distance from the anchor increased. For the lower embedment ratio ($\lambda = 3.2$), the contact force networks for the loose and dense assemblies were quite similar. However, at the larger embedment ratio ($\lambda = 7.2$), there were significant differences in the contact force networks for the loose and dense assemblies. Contact forces above the plate anchor were larger in the dense assembly than in the loose assembly. At higher embedment ratios, the difference in self-weight of the overburden for the loose and dense assemblies became apparent, causing the observed differences in the contact force networks.

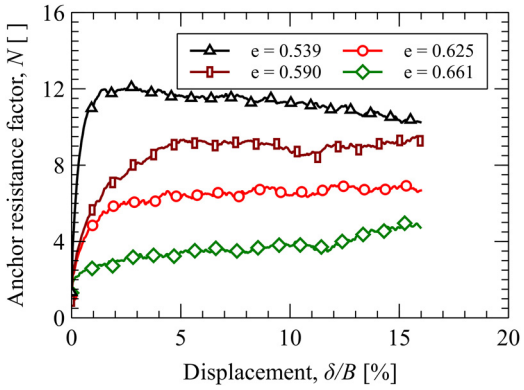

Fig. 11. Anchor resistance factor versus relative displacement for assemblies with different void ratios.

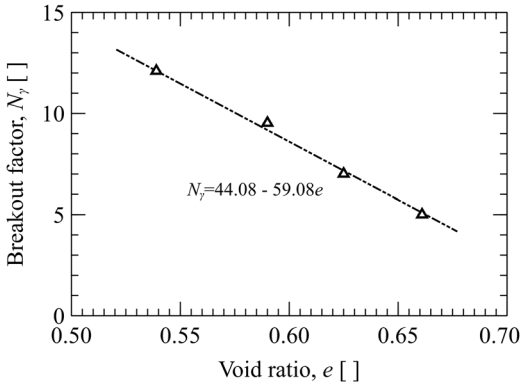

Fig. 12. Variation of breakout factor with the void ratio of the surrounding matrix.

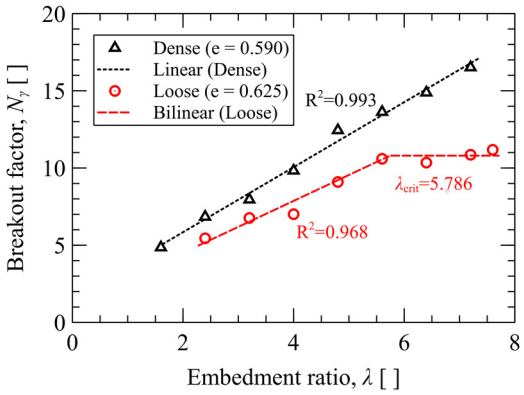

Fig. 13. Breakout factor as a function of embedment ratio.

Three-dimensional particle vertical velocity (in the vertical direction) color maps of the granular assemblies after the anchor is fully mobilized for loose and dense assemblies and different embedment ratios are presented in Fig. 15. Particles with velocities larger than 0.004 m/s are colored according to their velocities. Particles with velocities below this threshold are not presented. The color maps for the shallow embedment depth ($\lambda = 3.2$) reveal that the size of the influence zone in the dense assembly was larger and particles had larger velocities, particularly near the surface. In all cases considered, the region of particle movement took the shape of an inverted conical frustum after the anchor was fully mobilized. At

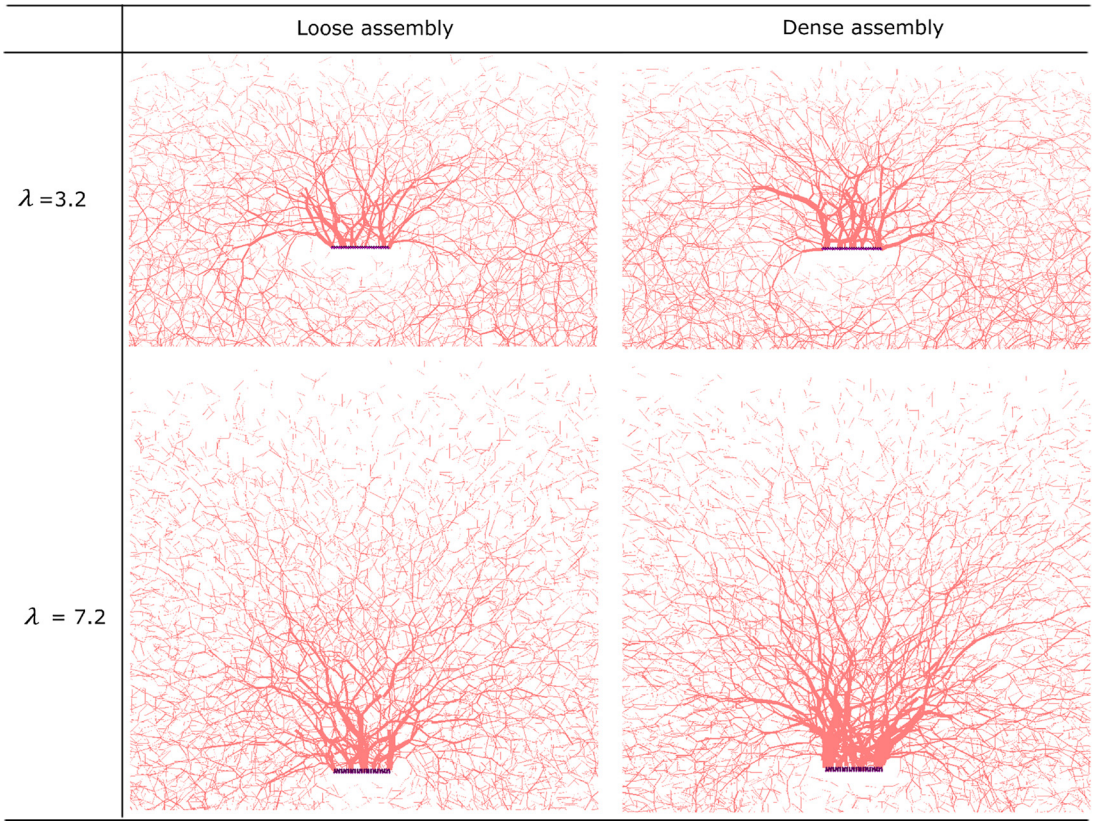

Fig. 14. Contact force network of loose and dense assemblies for two selected embedment ratios. Contact normal forces were normalized by 200 N for $\lambda = 3.2$ and 600 N for $\lambda = 7.2$.

the higher embedment ratio ($\lambda = 7.2$), the influence zone was substantially larger for the dense assembly. For both depths of embedment, it is clear that more particles were engaged in shear resistance in the dense assemblies than in the loose assemblies. This is due in part to the increased size of the zone of influence, but significantly, it is also because of the relative number of particles within the influence zone that were actively engaged.

Effects of Anchor Size

We considered the effects of changing anchor plate size on the breakout factor at two different soil densities: dense ($e = 0.590$) and loose ($e = 0.625$). The results indicate that breakout factor decreased with increasing anchor size for both assembly densities considered (Fig. 16). Dickin (1988) reported similar trends for experimental studies of anchor size effects on breakout factor. Although this initially seems counterintuitive, it is important to remember that breakout factor is a reflection of anchor holding efficiency, not capacity, because it is failure load normalized by the gravitational force supplied by the overburden material. Thus, a lower breakout factor corresponds to less holding efficiency. In general, the rate of increase in holding capacity as anchor size increased was not as great as the rate of increase in the overburden load associated with the larger cross-sectional area [i.e., Eq. (1)].

Failure Mechanism

Three primary failure mechanisms have been postulated by previous researchers. Fig. 17(a) presents the first failure surface, a frictional cylinder first proposed by Majer (1955) (Liu et al. 2012) and called the vertical slip surface model (VSSM). In the VSSM, the holding capacity is the soil weight above the plate anchor multiplied by the frictional resistance along the failure surface. This assumed failure mechanism is generally considered too conservative (e.g., Ilamparuthi et al. 2002; Liu et al. 2012). The second failure mechanism (Mors 1959), presented in Fig. 17(b), assumes a conical frustum extending above the plate anchor from its edge to the soil surface with an inclination of θ to the vertical. Murray and Geddes (1987) suggested that θ ranges from $\phi'/2$ to ϕ'. The holding capacity is calculated to be the weight of the conical frustum. This failure mechanism is also generally considered to be too conservative (Ilamparuthi et al. 2002) for shallow anchors because it neglects the frictional resistance along the failure surface. For deep anchors, however, it overestimates holding capacity because the failure surface for deep anchors does not extend to the free surface (Liu et al. 2012). The third failure mechanism [Fig. 17(c)] is a curved slip plane that extends from the anchor edges to the free surface with an initial inclination of $45^\circ - \phi'/2$, as observed by Balla (1961) through half-cut model experiments. Balla (1961) simplified the curved arc to a circular arc with a radius of $(H_0 - h)/\sin(45^\circ + \phi'/2)$, where H_0 is the embedment depth, and h is the anchor thickness. Although the three failure mechanisms discussed here are the most widely accepted, other failure surfaces have been postulated. Matsuo (1967) and Khadilkar et al. (1971) assumed that the rupture geometry is a logarithmic spiral and a tangential plane inclines at $45^\circ - \phi'/2$ to the surface. However, this method does not consider the frictional force in the required direction and is typically considered to be invalid (Murray and Geddes 1987). Chattopadhyay and Pise (1986) assumed an exponential equation to describe the failure surface and applied limit-equilibrium analyses, and found that a critical embedment depth exists, beyond which the breakout factor

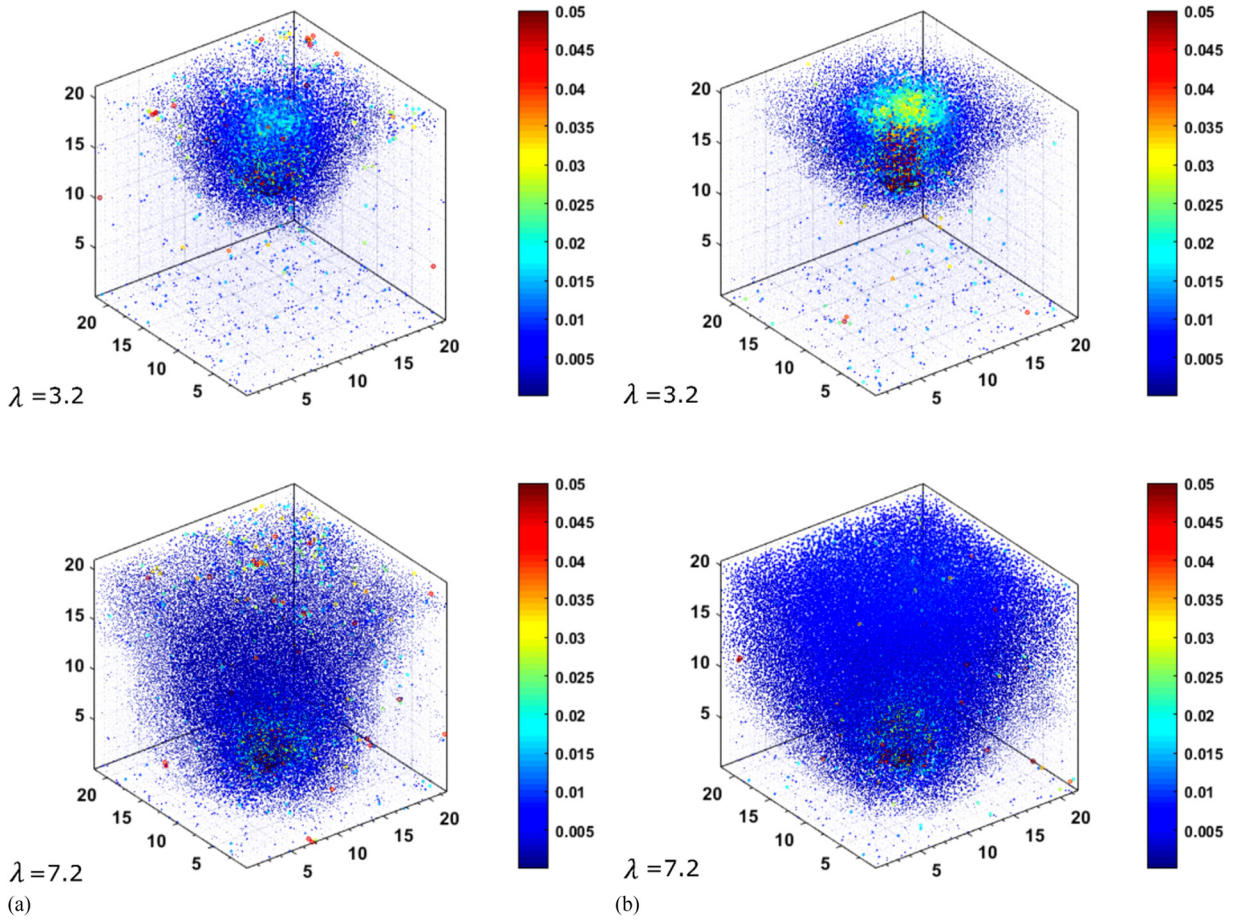

Fig. 15. Particle velocity (m/s) color map for two embedment ratios: (a) loose assembly; and (b) dense assembly.

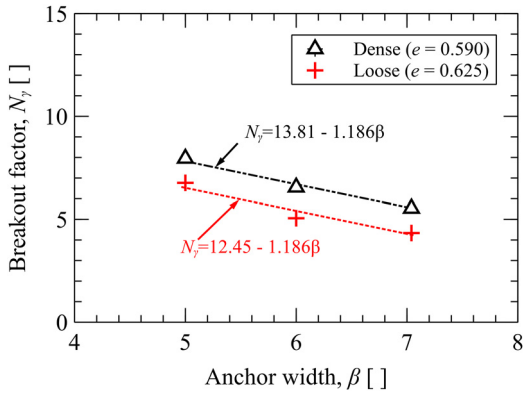

Fig. 16. Breakout factor under different anchor sizes ($\lambda = 4.8$), where $\beta = B/d_{50}$.

is constant, consistent with previously reported findings (e.g., Vesić 1971; Das and Seeley 1975). These additional failure mechanisms are specific examples of the mechanisms seen in Fig. 17. Regardless of the specific assumptions made, the three aforementioned mechanisms consist of two components: (1) the soil weight in the volume bounded by the plate anchor and the assumed failure surface, and (2) the frictional force on the failure surface.

We now consider discrete failure mechanisms that occurred in the DEM simulations through analysis of particle relative displacements and velocities and contact force transfer and diffusion during the pullout. Fig. 18 presents the contact force networks before and after full anchor mobilization on a slice cut from the three-dimensional assembly through the center. Fig. 18(a) reveals that before anchor movement, contact force magnitudes showed a gravitational gradient. Contact forces were uniformly distributed, also seen in Fig. 19. After anchor mobilization, larger contact forces occurred on the top of the plate anchor [Fig. 18(b)], and contact forces were redistributed in the assembly with a preferred spatial distribution. Contact force values immediately above the plate anchor clearly increased due to anchor mobilization and had much larger magnitudes than those due to body forces alone. This is micromechanical evidence that gravitational forces above the plate were not the only factor providing holding capacity (i.e., $N_\gamma > 1$). Clearly, the friction force acting on the failure surface contributed significantly to the holding resistance of the plate anchor.

The magnitudes of the contact forces were narrowly distributed prior to anchor uplift, as seen in Fig. 19, where normalized contact force is defined as the contact normal force divided by the mean contact normal force in the assembly prior to uplift. Fig. 19 indicates that the normalized contact normal force ranged from nearly 0 to 10 for the anchor before uplift and varied from nearly 0 to 60 during uplift. The mobilization of the plate anchor compressed the assembly above the anchor, thus increasing the contact normal forces.

Fig. 20 presents a slice of particle velocities for the same dense and loose assemblies considered in Fig. 15. As seen in Figs. 20 and 15, particle velocities had a pronounced gradient from immediately above the anchor to their surrounding neighbors. Particles in contact with the plate anchor were directly influenced by plate mobilization.

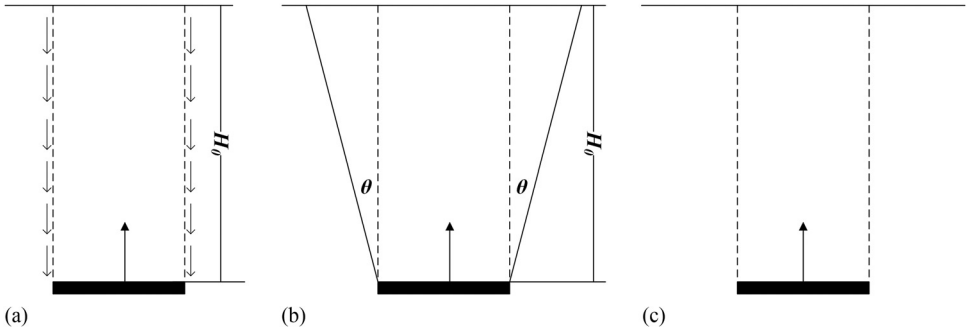

Fig. 17. Plate anchor failure mechanism diagrams: (a) VSSM; (b) truncated cone; and (c) curved failure surface.

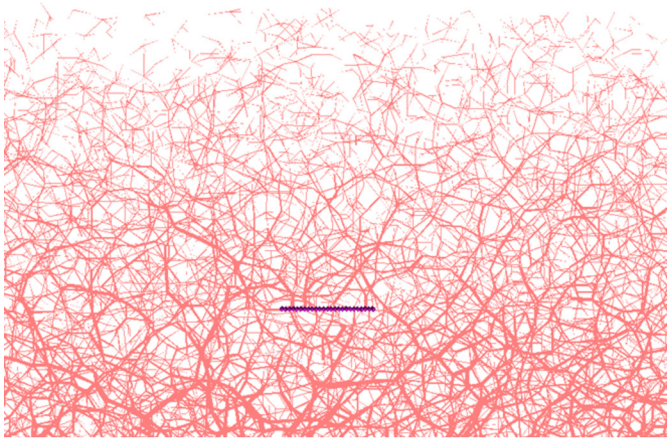

(a)

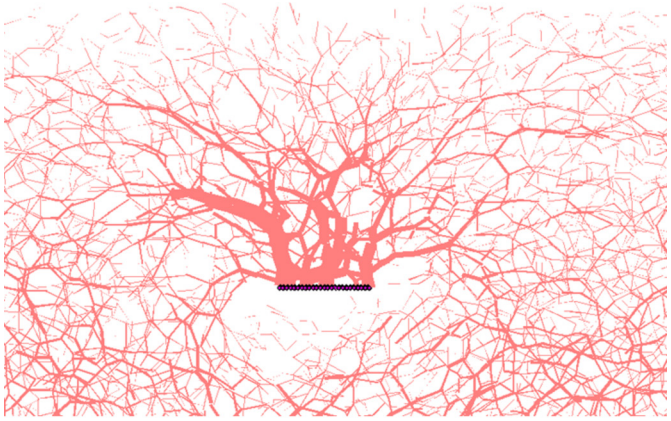

(b)

Fig. 18. Contact force chain development for an embedment ratio of $\lambda = 3.2$: (a) before; and (b) after full anchor mobilization. Contact normal forces were normalized by 200 N before pullout and 600 N after full mobilization.

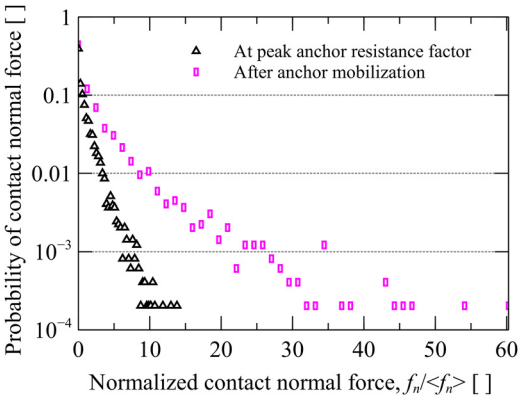

Fig. 19. Contact normal force distribution in the granular assembly. Forces were normalized by the mean contact normal force in the assembly.

Due to interparticle friction (for nonspherical particles, there would also be particle interlocking), mobilization of particles resulted in friction forces along the failure surface. Failure was observed where particle velocities exhibited an abrupt change in magnitude: this was the location of the shear band. The localization initially occurred as particle velocities diffused from the plate anchor to the surface and then continuously existed as anchor pullout continued.

The failure mechanisms for the loose and dense assemblies were different. Fig. 21 presents the velocity fields for dense and loose assemblies at the same displacement. The influence zone was markedly larger for the dense assembly. For a shallow anchor in the loose assembly, the failure surface was not as clearly defined at the top of the assembly compared to the dense assembly, implying greater particle rearrangement in the loose assembly (consistent with diffuse failure) relative to the dense assembly [implying rigid block sliding along the shear band (Evans and Frost 2010)]. Significant particle motions in the loose assembly occurred in a bulb-shaped influence zone; similar behavior was reported by Liu et al. (2012) via experimental tests.

Anchor Response to Cyclic Loading

Plate anchors are subjected to cyclic wave loading for offshore structures (e.g., WECs, oil platforms). Granular soil behavior under cyclic loading was briefly considered here. In the simulations, the applied cyclic loads were based on the maximum holding resistance (P_{peak}) generated from the static pullout simulations discussed earlier (Fig. 22). Cyclic loading involved four steps from $0.4P_{peak}$ to $1.2P_{peak}$, where P_{peak} is the maximum holding resistance under static loading for the same embedment depths.

Fig. 23 presents the anchor relative vertical displacement for the different stages of cyclic loading. Relative vertical displacement is defined as the vertical displacement normalized by anchor width, expressed as a percentage. According to Lesny and Hinz (2009), soils in contact with cyclically loaded monopole foundations exhibit three stages of behavior: (1) shake down, (2) stabilization, and (3) progressive failure. Fig. 23 presents the shake-down behavior when the loading magnitudes were $0.4P_{peak}$ and stabilization was

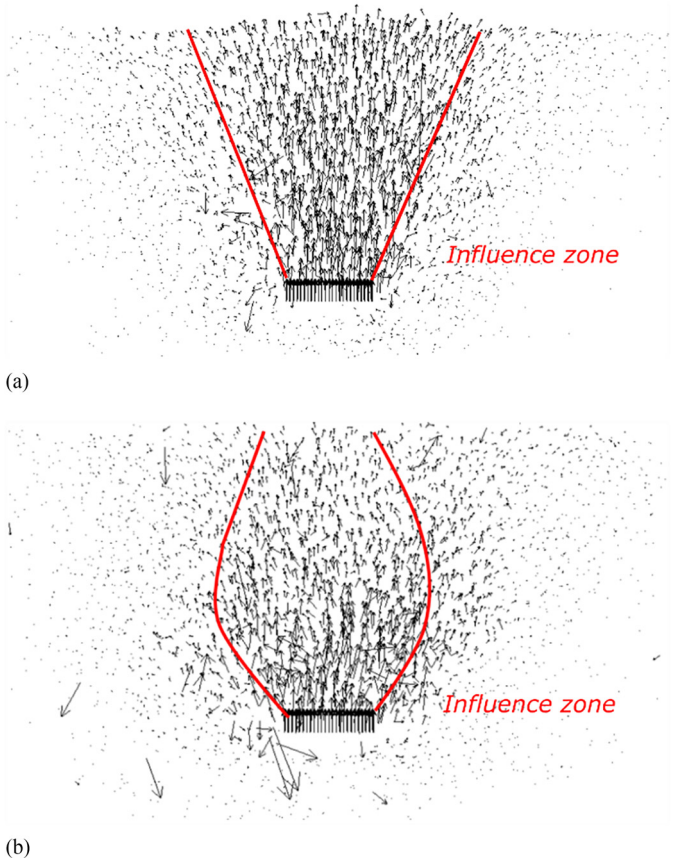

Fig. 20. Particle velocity vector ($\lambda = 3.2$): (a) dense assembly; and (b) loose assembly.

observed when the cyclic loading was $0.8P_{peak}$ or $1.0P_{peak}$. The soil failed when the cyclic loading was $1.2P_{peak}$. Relative vertical displacement increments increased with increasing cyclic loading.

A virtual box with dimensions of $0.3L \times 0.3W \times 0.2H$ immediately above the plate anchor was used to compute the stress tensor and mean stress during cyclic loading. The stress tensor was obtained from the contact information inside the virtual box, as seen in Eq. (12) (e.g., O'Sullivan 2011)

$$\begin{bmatrix} \sigma_{xx} & \sigma_{xy} & \sigma_{xz} \\ \sigma_{yx} & \sigma_{yy} & \sigma_{yz} \\ \sigma_{zx} & \sigma_{zy} & \sigma_{zz} \end{bmatrix} = \frac{1}{V} \begin{bmatrix} \sum_{c=1}^{N_{c,V}} f_x^c l_x^c & \sum_{c=1}^{N_{c,V}} f_x^c l_y^c & \sum_{c=1}^{N_{c,V}} f_x^c l_z^c \\ \sum_{c=1}^{N_{c,V}} f_y^c l_x^c & \sum_{c=1}^{N_{c,V}} f_y^c l_y^c & \sum_{c=1}^{N_{c,V}} f_y^c l_z^c \\ \sum_{c=1}^{N_{c,V}} f_z^c l_x^c & \sum_{c=1}^{N_{c,V}} f_z^c l_y^c & \sum_{c=1}^{N_{c,V}} f_z^c l_z^c \end{bmatrix} \tag{12}$$

where $N_{c,V}$ = total number of contacts in the volume (V); $[f_x\ f_y\ f_z]$ = force vector for contact c; and $[l_x\ l_y\ l_z]$ = branch vector for contact c. From the first invariant of Cauchy's stress tensor, the mean stress is obtained by Eq. (13)

$$p = \frac{tr\boldsymbol{\sigma}}{3} = -\frac{I_1}{3} = \frac{\sigma_{xx} + \sigma_{yy} + \sigma_{zz}}{3} \tag{13}$$

where p = mean stress; and I_1 = first invariant of the stress tensor.

The mean stress in the virtual box when the embedment ratio was 7.2 is presented in Fig. 24. Normalized mean stress in Fig. 24 is defined as the mean stress obtained from the stress tensor divided by the vertical geostatic stress(σ_z). Given the internal friction angle of 24°, the lateral earth-pressure coefficient at rest was $K_0 = (1 - \sin(24^\circ)) = 0.593$, the active earth-pressure coefficient was $K_a = (1 - \sin(24^\circ))/(1 + \sin(24^\circ)) = 0.422$, and the passive earth-pressure coefficient was $K_p = (1 + \sin(24^\circ))/(1 - \sin(24^\circ)) = 2.37$. Fig. 24 indicates that the normalized mean stress was initially

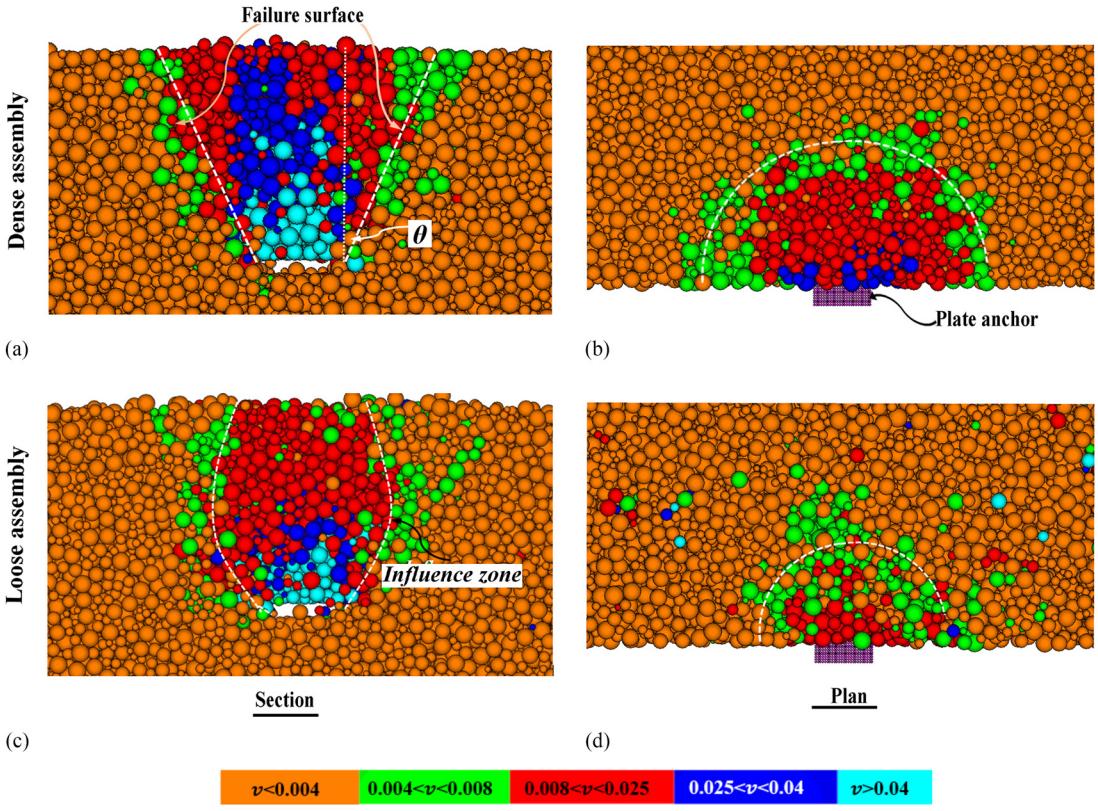

Fig. 21. Failure mechanism inferred from particle velocities: (a and b) dense assembly; and (c and d) loose assembly ($\lambda = 3.2$).

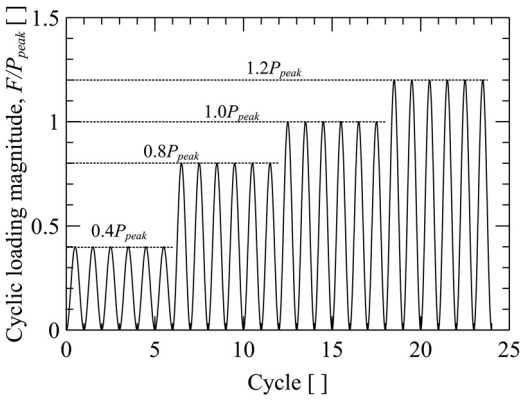

Fig. 22. Cyclic loads. Cyclic loading ratio is defined as the ratio of applied load to the maximum anchor holding force under static loading condition.

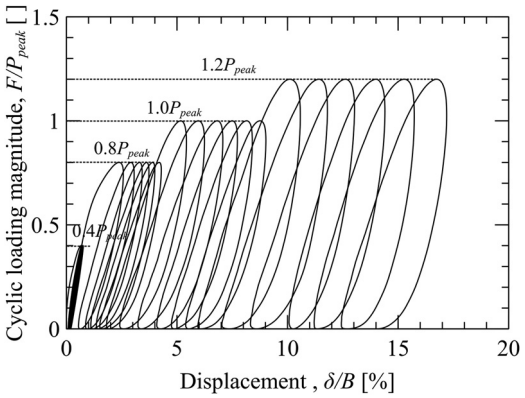

Fig. 23. Magnitude of cyclic load as a function of relative vertical displacement ($\lambda = 7.2$ dense assembly).

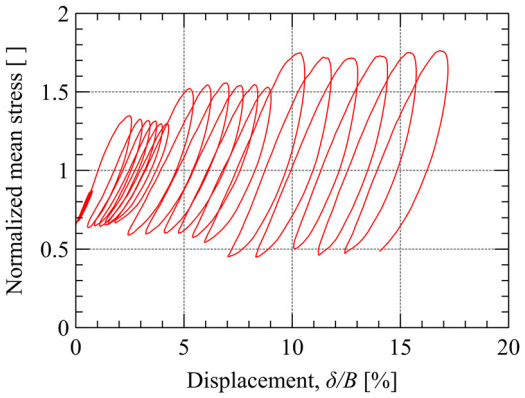

Fig. 24. Mean stress of the considered virtual box along with relative vertical displacement ($\lambda = 7.2$ dense assembly).

0.65 and ranged from 0.45 to 1.77 during the cyclic loading–unloading process. The granular assembly was capable of supporting larger loading magnitudes ($1.2P_{peak}$) during cyclic loading than the static monotonic loading capacity, consistent with the recent findings by Chow et al. (2015). Results showed that there was no stress relaxation under small cyclic loads; however, larger loads mobilized significant passive resistance, even if not fully, and the corresponding unloading partially mobilized the active resistance

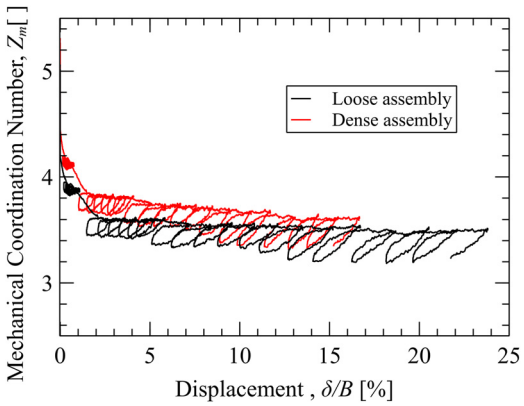

Fig. 25. Evolution of mechanical coordination number with cyclic loading for loose and dense assemblies with an embedment ratio of $\lambda = 7.2$.

and allowed stress relaxation. The normalized mean stress varied from approximately the active to the passive earth-pressure coefficient.

To further investigate this behavior, we considered the evolution of coordination number under cyclic loading for different assembly densities. Mechanical coordination number (Thornton 2010) is defined as $Z_m = (2C - N_1)/(N_p - N_1 - N_0)$, where Z_m is the mechanical coordination number; C is the number of contacts in the measurement volume; N_1 and N_0 are the number of particles with one or zero contacts, respectively; and N_p = number of particles. Mechanical coordination number versus relative vertical displacement for dense and loose assemblies for the same embedment ratio ($\lambda = 7.2$) are presented in Fig. 25. For similar cyclic loading ratios and numbers of cycles, relative vertical displacement in the loose assembly (24%) was larger than for the dense assembly (17%). During cyclic loading, the mechanical coordination numbers varied but underwent shake down to relatively constant values at the fully loaded and fully unloaded states. These steady states were nearly the same for both the initially dense and initially loose assemblies, illustrating the homogenizing effects of shear. This is microscale evidence of momentary instability during the load–unload cycles.

Conclusions

System- and particle-scale analyses of plate anchors embedded into granular soils based on DEM are presented in this paper. We considered both anchor properties (e.g., embedment depth, roughness, size) and soil properties (e.g., density). The results were reported as dimensionless breakout factors as functions of embedment ratio, relative density, anchor size, and anchor roughness. Consistency in results across DEM simulations, experimental tests, and empirical equations was demonstrated. Anchor failure mechanisms were analyzed by investigating particle-scale response to anchor uplift. The following conclusions may be drawn from the findings presented in this paper:

1. Breakout factor linearly increased with the increase of embedment ratio at relatively shallow embedment depths for both dense and loose granular assemblies. However, a critical breakout factor, beyond which increasing embedment depth is no longer efficient, was observed for the loose assembly. The DEM simulation results were consistent with experimental tests and empirical equations for similar internal friction.

Int. J. Geomech., 2019, 19(4): 04019004

2. Anchor roughness had little influence on the resistance of plate anchors: the breakout factors were similar for all of the selected anchor roughnesses. The results showed that breakout factor decreased with anchor size for both dense and loose assemblies.
3. Contact forces attenuated from the plate anchor up to the surface. There was no significant difference in the contact force network for varying embedment ratios. However, for a larger embedment ratio, there was a marked difference between loose and dense assemblies. Contact forces above the plate anchor were larger and more concentrated in the dense assembly than in the loose assembly. Body forces combined with the uplifting anchor to contribute to the strong contact forces above the plate anchor.
4. Observation of microscale failure mechanisms provided insight into the system-scale manifestation of failure in the assembly. Particle relative displacement, velocity, and contact force transfer during uplift all illustrated the differences in failure mechanisms across simulations. The failure mechanisms for loose and dense assemblies were demonstrably different. For a shallow anchor in a loose assembly, granular soil mobilization did not fully extend to the surface as clearly as in the dense assembly. Significant particle rearrangement occurred in a bulb-shaped influence zone in the loose assembly (diffuse failure), whereas a well-defined shear surface developed in the dense assembly.
5. These differences in failure mechanisms across embedment ratios and soil densities imply that a single empirical or semianalytical equation is likely not appropriate for robustly quantifying pullout resistance of plate anchors in granular soils.
6. There was no stress relaxation under small cyclic loading; however, larger applied loads mobilized passive resistance, and the corresponding unloading mobilized active resistance. Normalized mean stress varied from approximately the active earth-pressure state to approximately the passive earth-pressure state. The plate anchor had a higher holding capacity during cyclic loading than under monotonic loading.
7. During cyclic loading, the mechanical coordination number experienced shake down to a constant range of values (i.e., between fully loaded and fully unloaded) that was effectively independent of the initial state. This provides microscale evidence of steady-state behavior and implies that, although monotonic resistance immediately after anchor installation is a strong function of soil state, the long-term behavior may not be.

Acknowledgments

This material is based upon work supported by the Department of Energy under Award DE-FG36-08GO18179. This paper was prepared as an account of work sponsored by an agency of the United States Government. Neither the United States Government nor any agency thereof, nor any of their employees, makes any warranty, expressed or implied, or assumes any legal liability or responsibility for the accuracy, completeness, or usefulness of any information, apparatus, product, or process disclosed, or represents that its use would not infringe privately owned rights. The views and opinions of the authors expressed herein do not necessarily state or reflect those of the United States Government or any agency thereof.

References

Athani, S., P. Kharel, D. Airey, and P. Rognon. 2017. "Grain-size effect on uplift capacity of plate anchors in coarse granular soils." *Géotechnique Lett.* 7 (2): 167–173. https://doi.org/10.1680/jgele.17.00002.

Balla, A. 1961. "The resistance to breaking out of mushroom foundations for pylons." In *Proc., 5th Int. Conf. on Soil Mechanics and Foundation Engineering*, 569–576. Paris: Dunod.

Basudhar, P. K., and D. N. Singh. 1994. "A generalized procedure for predicting optimal lower bound break-out factors of strip anchors." *Géotechnique* 44 (2): 307–318. https://doi.org/10.1680/geot.1994.44.2.307.

Belheine, N., J. P. Plassiard, F.-V. Donzé, F. Darve, and A. Seridi. 2009. "Numerical simulation of drained triaxial test using 3-D discrete element modeling." *Comput. Geotech.* 36 (1–2): 320–331. https://doi.org/10.1016/j.compgeo.2008.02.003.

Chattopadhyay, B. C., and P. J. Pise. 1986. "Breakout resistance of horizontal anchors in sand." *Soils Found.* 26 (4): 16–22. https://doi.org/10.3208/sandf1972.26.4_16.

Chow, S. H., C. D. O'Loughlin, R. Corti, C. Gaudin, and A. Diambra. 2015. "Drained cyclic capacity of plate anchors in dense sand: Experimental and theoretical observations." *Géotechnique Lett.* 5 (2): 80–85. https://doi.org/10.1680/geolett.15.00019.

Cundall, P. A., and O. D. L. Strack. 1979. "A discrete numerical model for granular assemblies." *Géotechnique* 29 (1): 47–65. https://doi.org/10.1680/geot.1979.29.1.47.

Das, B. M., and G. R. Seeley. 1975. "Breakout resistance of shallow horizontal anchors." *J. Geotech. Eng. Div.* 101 (9): 999–1003.

Das, B. M., E. C. Shin, R. N. Dass, and M. T. Omar. 1994. "Suction force below plate anchors in soft clay." *Mar. Georesour. Geotechnol.* 12 (1): 71–81. https://doi.org/10.1080/10641199409388255.

Dickin, E. A. 1988. "Uplift behavior of horizontal anchor plates in sand." *J. Geotech. Eng.* 114 (11): 1300–1317. https://doi.org/10.1061/(ASCE)0733-9410(1988)114:11(1300).

Dickin, E. A., and M. Laman. 2007. "Uplift response of strip anchors in cohesionless soil." *Adv. Eng. Software* 38 (8–9): 618–625. https://doi.org/10.1016/j.advengsoft.2006.08.041.

Dyson, A. S., and P. G. Rognon. 2014. "Pull-out capacity of tree root inspired anchors in shallow granular soils." *Géotechnique Lett.* 4 (4): 301–305. https://doi.org/10.1680/geolett.14.00061.

Evans, T. M., and J. D. Frost. 2010. "Multiscale investigation of shear bands in sand: Physical and numerical experiments." *Int. J. Numer. Anal. Methods Geomech.* 34 (15): 1634–1650.

Evans, T. M., and J. G. Kress. 2011. "Discrete simulations of particulate-structure interactions." In *GeoFrontiers 2011: Advances in Geotechnical Engineering*, Geotechnical Special Publication 211, 4252–4262. Reston, VA: Geo-Institute.

Evans, T. M., and J. R. Valdes. 2011. "The microstructure of particulate mixtures in one-dimensional compression: Numerical studies." *Granular Matter* 13 (5): 657–669. https://doi.org/10.1007/s10035-011-0278-z.

Frost, J. D., J. T. DeJong, and M. Recalde. 2002. "Shear failure behavior of granular–continuum interfaces." *Eng. Fract. Mech.* 69 (17): 2029–2048. https://doi.org/10.1016/S0013-7944(02)00075-9.

Frost, J. D., G. Hebeler, T. M. Evans, and J. DeJong. 2004. "Interface behavior of granular soils." In *Proc., Engineering, Construction, and Operations in Challenging Environments*, 65–72. Reston, VA: ASCE.

Frydman, S., and I. Shaham. 1989. "Pullout capacity of slab anchors in sand." *Can. Geotech. J.* 26 (3): 385–400. https://doi.org/10.1139/t89-053.

Gao, G., and M. A. Meguid. 2018. "On the role of sphericity of falling rock clusters—Insights from experimental and numerical investigations." *Landslides* 15 (2): 219–232. https://doi.org/10.1007/s10346-017-0874-z.

Gaudin, C., C. D. O'Loughlin, M. F. Randolph, and A. C. Lowmass. 2006. "Influence of the installation process on the performance of suction embedded plate anchors." *Géotechnique* 56 (6): 381–391. https://doi.org/10.1680/geot.2006.56.6.381.

Holtz, R. D., W. D. Kovacs, and T. C. Sheahan. 2011. *An introduction to geotechnical engineering*. 2nd ed. Upper Saddle River, NJ: Prentice Hall.

Ilamparuthi, K., E. A. Dickin, and K. Muthukrisnaiah. 2002. "Experimental investigation of the uplift behaviour of circular plate anchors embedded in sand." *Can. Geotech. J.* 39 (3): 648–664. https://doi.org/10.1139/t02-005.
Itasca Consulting Group. 2008. *PFC3D: Particle flow code in three dimensions v4.0.* Minneapolis: Itasca Consulting Group.
Khadilkar, B. S., A. K. Paradkar, and Y. S. Golait. 1971. "Study of rupture surface and ultimate resistance of anchor foundations." In Vol. 1 of *Proc., 4th Asian Regional Conf. on Soil Mechanics and Foundation Engineering*, 121–127. Bangkok, Thailand: AIT.
Kress, J. G., and T. M. Evans. 2010. "Analysis of pile behavior in granular soils using DEM." In *Proc., 35th Annual Deep Foundations Institute Annual Conf.* Hawthorne, NJ: Deep Foundations Institute.
Kumar, J., and K. M. Kouzer. 2008a. "Vertical uplift capacity of a group of shallow horizontal anchors in sand." *Géotechnique* 58 (10): 821–823. https://doi.org/10.1680/geot.2008.58.10.821.
Kumar, J., and K. M. Kouzer. 2008b. "Vertical uplift capacity of horizontal anchors using upper bound limit analysis and finite elements." *Can. Geotech. J.* 45 (5): 698–704. https://doi.org/10.1139/T08-005.
Lesny, K., and P. Hinz. 2009. "Design of monopile foundations for offshore wind energy converters." In *Contemporary topics in deep foundations*, 512–519. Reston, VA: ASCE.
Liu, J., M. Liu, and Z. Zhu. 2012. "Sand deformation around an uplift plate anchor." *J. Geotech. Geoenviron. Eng.* 138 (6): 728–737. https://doi.org/10.1061/(ASCE)GT.1943-5606.0000633.
Majer, J. 1955. "Zur berechnung von zugfundamenten." [In German.] *Osterreichister Bauzeitschift* 10 (5): 85–90.
Matsuo, M. 1967. "Study of uplift resistance of footing (I)." *Soils Found.* 7 (4): 1–37. https://doi.org/10.3208/sandf1960.7.4_1.
Merifield, R. S., and S. W. Sloan. 2006. "The ultimate pullout capacity of anchors in frictional soils." *Can. Geotech. J.* 43 (8): 852–868. https://doi.org/10.1139/t06-052.
Meyerhof, G. G. 1951. "The ultimate bearing capacity of foundations." *Géotechnique* 2 (4): 301–332. https://doi.org/10.1680/geot.1951.2.4.301.
Meyerhof, G. G., and J. I. Adams. 1968. "The ultimate uplift capacity of foundations." *Can. Geotech. J.* 5 (4): 225–244. https://doi.org/10.1139/t68-024.
Mors, H. 1959. "Das verhalten von mastgruendungen bei zugbeansprüchung." [In German.] *Bautechnik* 36 (10): 367–378.
Mühlhaus, H., and I. Vardoulakis. 1987. "The thickness of shear bands in granular materials." *Géotechnique* 37 (3): 271–283. https://doi.org/10.1680/geot.1987.37.3.271.
Murray, E. J., and J. D. Geddes. 1987. "Uplift of anchor plates in sand." *J. Geotech. Eng.* 113 (3): 202–215. https://doi.org/10.1061/(ASCE)0733-9410(1987)113:3(202).
Murray, E. J., and J. D. Geddes. 1989. "Resistance of passive inclined anchors in cohesionless medium." *Géotechnique* 39 (3): 417–431.
O'Sullivan, C. 2011. *Particulate discrete element modelling: A geomechanics perspective.* New York: Spon Press.
Ovesen, N. K. 1981. "Centrifuge tests to determine the uplift capacity of anchor slabs in sand." In Vol. I of *Proc., 10th Int. Conf. on Soil Mechanics and Foundation Engineering*, 717–722. Rotterdam: A.A. Balkema.
Randolph, M., and S. Gourvenec. 2011. *Offshore geotechnical engineering.* Boca Raton, FL: CRC Press.
Rao, K. S. S., and J. Kumar. 1994. "Vertical uplift capacity of horizontal anchors." *J. Geotech. Eng.* 120 (7): 1134–1147. https://doi.org/10.1061/(ASCE)0733-9410(1994)120:7(1134).
Rowe, R. K., and E. H. Davis. 1982. "The behaviour of anchor plates in sand." *Géotechnique* 32 (1): 25–41. https://doi.org/10.1680/geot.1982.32.1.25.
Song, Z., Y. Hu, and M. F. Randolph. 2008. "Numerical simulation of vertical pullout of plate anchors in clay." *J. Geotech. Geoenviron. Eng.* 134 (6): 866–875. https://doi.org/10.1061/(ASCE)1090-0241(2008)134:6(866).
Thornton, C. 2010. "Quasi-static simulations of compact polydisperse particle systems." *Particuology* 8 (2): 119–126. https://doi.org/10.1016/j.partic.2009.07.007.
Uesugi, M., and H. Kishida. 1986. "Frictional resistance at yield between dry sand and mild steel." *Soils Found.* 26 (4): 139–149. https://doi.org/10.3208/sandf1972.26.4_139.
Valent, P. J., R. J. Taylor, J. M. Atturio, and R. M. Beard. 1979. "Single anchor holding capacities for ocean thermal energy conversion (OTEC) in typical deep sea sediments." *Ocean Eng.* 6 (1–2): 169–245. https://doi.org/10.1016/0029-8018(79)90005-2.
Vesić, A. S. 1971. "Breakout resistance of objects embedded in ocean bottom." *J. Soil Mech. & Foundations Div.* 97 (9): 1183–1205.
White, D. J., C. Y. Cheuk, and M. D. Bolton. 2008. "The uplift resistance of pipes and plate anchors buried in sand." *Géotechnique* 58 (10): 771. https://doi.org/10.1680/geot.2008.3692.
Yu, L., J. Liu, X. J. Kong, and Y. Hu. 2011. "Numerical study on plate anchor stability in clay." *Géotechnique* 61 (3): 235–246. https://doi.org/10.1680/geot.8.P.071.
Zhang, N., and T. M. Evans. 2016. "Towards the anchoring of marine hydrokinetic energy devices: Three-dimensional discrete element method simulations of interface shear." In *Proc., Geo-Chicago 2016: Geotechnics for Sustainable Energy*, Geotechnical Special Publication 270, 503–512. Reston, VA: ASCE.
Zhang, N., and T. M. Evans. 2017. "Offshore anchor penetration in sands—Granular simulations." In *Proc., GeoFrontiers 2017: Foundations*, Geotechnical Special Publication 279, 132–142. Reston, VA: ASCE.
Zhang, N., and T. M. Evans. 2018. "Three dimensional discrete element method simulations of interface shear." *Soils Found.* 58 (4): 941–956. https://doi.org/10.1016/j.sandf.2018.05.010.
Zhao, S., T. Evans, and X. Zhou. 2018. "Effects of curvature-related DEM contact model on the macro- and micro-mechanical behaviours of granular soils." *Géotechnique* 68 (12): 1085–1098. https://doi.org/10.1680/jgeot.17.P.158.
Zhao, S., N. Zhang, X. Zhou, and L. Zhang. 2017. "Particle shape effects on fabric of granular random packing." *Powder Technol.* 310: 175–186. https://doi.org/10.1016/j.powtec.2016.12.094.
Zhao, X., and T. M. Evans. 2009. "Discrete simulations of laboratory loading conditions." *Int. J. Geomech.* 9 (4): 169–178. https://doi.org/10.1061/(ASCE)1532-3641(2009)9:4(169).